ACS Macro Letters

pubs.acs.org/macroletters Letter

Thermal Stability of π-Conjugated *n*-Ethylene-Glycol-Terminated Quaterthiophene Oligomers: A Computational and Experimental Study

Mayank Misra, Ziwei Liu, Ban Xuan Dong, Shrayesh N. Patel, Paul F. Nealey, Christopher K. Ober, and Fernando A. Escobedo*

Cite This: *ACS Macro Lett.* 2020, 9, 295−300 Read Online

ACCESS | Metrics & More | Article Recommendations | Supporting Information

ABSTRACT: This work represents a joint computational and experimental study on a series of *n*-ethylene glycol (PEO*n*)-terminated quaterthiophene (4T) oligomers for $1 < n < 10$ to elucidate their self-assembly behavior into a smectic-like lamellar phase. This study builds on an earlier study for $n = 4$ that showed that our model predictions were consistent with experimental data on the melting behavior and structure of the lamellar phase, with the latter consisting of crystal-like 4T domains and liquid-like PEO4 domains. The present study aims to understand how the length of the terminal PEO*n* chains modulates the disordering temperature of the lamellar phase and hence the relative stability of the ordered structure. A simplified bilayer model, where the 4T domains are not explicitly described, is put forward to efficiently estimate the disordering effect of the PEO domains with increasing *n*; this method is first validated by correctly predicting that layers of alkyl (PE)-capped 4T oligomers (for $1 < n < 10$) stay ordered at room temperature. Both 4T-domain implicit and explicit model simulations reveal that the order−disorder temperature decreases with the length of the PEO capping chains, as the associated increase in conformational entropy drives a tendency toward disorder that overtakes the cohesive energy, keeping the ordered packing of the 4T domains.

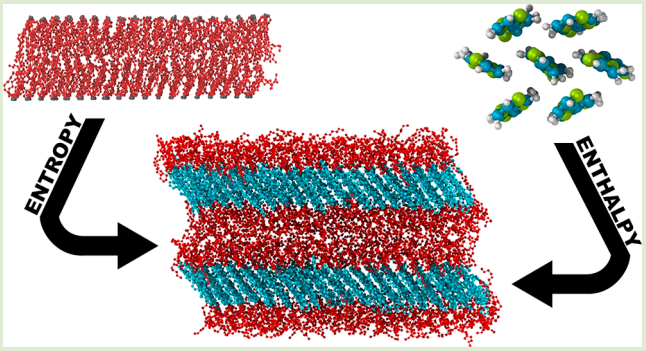

Mixed ionic/electronic conducting (MIEC) organic materials have garnered significant interest as ingredients for next-generation energy storage and separation devices. Their application ranges from membranes for pure oxygen production to thin wearable electronics.[1−5] Oligothiophene moieties, capable of electronic conduction, combined with poly(ethylene oxide)s (PEOs), capable of ionic conduction, have been identified as promising building blocks for mixed ionic/electronic conducting materials. Both components have been well studied individually and recognized as state-of-the-art materials for their respective conducting properties; however, the characterization of the structure and properties of materials where both of these components are chemically linked and co-assembled has only been explored in the case of polymers but not oligomers.[6−8] In our recent work, we explored this question by extensively analyzing linear 4T/PEO4 oligomers using experiments and molecular simulations.[9] These molecules have a central core of quarterthiophene rings (4T) connected on each side to butylene-ethylene oxide (PEO4) groups. We observed that these 4T/PEO4 molecules self-assemble into a smectic morphology where the 4T cores packed in a crystalline order similar to pure 4T, while the PEO4 tails formed intercalating layers with minimal interdigitation across layers. These results suggest that in this class of block oligomers the core thiophene rings determine molecular packing, while the capping linear oligomers have thermally mobile, relaxed conformations. Ashizawa et al.[10] observed an analogous layered morphology when studying similar linear block molecules consisting of a 4T core capped by alkyl chain (PE) chains (4T/PE*n*) (Figure 1(b)). While all the 4T/PE*n* materials studied were found to be well ordered at room conditions, it is conjectured that PEO units (replacing PE) would have a more disruptive effect on the ordered packing of 4T due to the lower melting points and less congruent packing of PEO chains relative to alkyl chains (for comparable molecular weights).[11,12] Here, we use molecular simulations to examine the effect of varying the number of units of PE and PEO on 4T to understand whether and how the capping chains may enhance or disrupt the smectic order. Since experimental studies of the phase behavior

Received: November 26, 2019
Accepted: February 3, 2020
Published: February 11, 2020

https://dx.doi.org/10.1021/acsmacrolett.9b00935
ACS Macro Lett. 2020, 9, 295−300

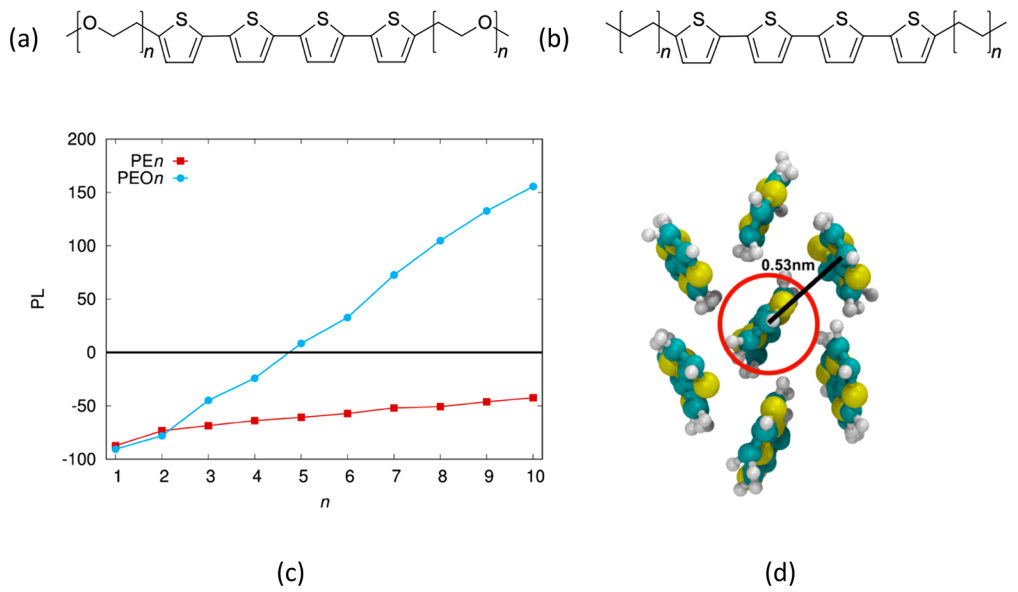

Figure 1. Chemical structure of (a) 4T/PE*n* and (b) 4T/PEO*n*. (c) Projected end-to-end distance metric for PE*n* and PEO*n* as a function of number of repeat units (n) at T = 300 K. The black line represents the nearest distance of 0.53 nm between two α carbons in the packed 4T layer shown in (d). The red circle denotes the critical projected end-to-end distance of oligomers in the *xy*-plane.

of the 4T/PEO*n* (Figure 1(a)) oligomer series are lacking, selected experiments for two of the 4T/PEO*n* oligomers are also described to validate the simulation findings.

To support our conjecture that the formation of intercalating layers for 4T/PEO*n* is primarily due to the packing of 4T crystals and not to a microphase separation driven by energetic (chemical) incompatibility between blocks as seen in amorphous block copolymers, we estimate the Flory−Huggins parameter (χ) based on the solubility parameter δ of individual components[13,14] for 4T/PEO4 using molecular dynamics (MD) simulations. All simulations were performed using LAMMPS,[15] with the modified force field used in our previous simulation for 4T/PEO4.[9] The calculated δ values for 4T and PEO4 are 20.84 $MPa^{1/2}$ and 21.0 $MPa^{1/2}$, respectively, which gives $\chi_{4T\text{-}PEO4} \sim 0.007$, i.e., a $0 < \chi N \ll 1$ for the 4T/PEO4 oligomer, indicative of very weak incompatibility. A diblock oligomer with this value of χN would be predicted to form a mixed disordered phase[16] at room temperature if both blocks were in an amorphous state. However, this is inconsistent with both experiments and simulations where a lamellar phase is observed. It is then clear that the ordering in 4T/PEO4 must be driven by the tendency of the 4T cores to crystallize, a process aided by both the $\pi-\pi$ interactions between thiophene rings[9,17,18] and the intrinsic backbone rigidity of the 4T units.

To probe how the structure of the PE and PEO tails may affect the stability of the lamellar phase, we first study their conformational behavior when grafted on a flat surface in the absence of 4T. The flat grafting surface is used as a minimalistic, simplified representation of the lamellar interface adjacent to the 4T domain. A key quantity affecting the conformational entropy of the grafted chain on a flat surface is chain-grafting density,[9] GD, defined as the number of chains per unit area. When GD is larger than the inverse square of the area projected by the radius of gyration of the oligomer chains on the *xy*-plane, $(1/R_{xy})^2$, individual chains start overlapping with adjacent chains, inducing strong steric hindrance and excluded-volume interactions, leading to more extended and stretched conformations of the brushes in the direction normal to the substrate. Hence, the chain stretching (as captured by the thickness of the PEO layer in 4T/PEO*n*) of the grafted chain is strongly affected by GD. Here, we mimic the chain lateral density of 4T/PE*n* by grafting $CH_3-(CH_2-CH_2)n$ (PE*n*) or $CH_3-(CH_2-CH_2-O)n$ (PEO*n*), where n = 1 to 10, to the α carbon of 4T, which gives a significantly high grafting density of 7.1 nm^{-2}. Thus, by keeping constant this GD, the flat surface (*xy*-plane) represents an idealization of the interface between 4T and PEO*n* in the 4T/PEO*n* system. We first create a single layer of 400 grafting sites at z = 0 in a simulation box with 7.5 × 7.5 × 12 nm. Note that the box is significantly larger along the *z*-axis to avoid periodic interactions in that direction and thus initially creates a large interlayer vacuum. Subsequently, the PEO*n* chains are grown along the positive *z*-axis direction from the grafting points. The nonbonded, bond, and angle potential parameters between grafting points and grafted carbon PEO*n* are the same as those of the α carbon in 4T and the α carbon in PEO. To prevent chains from going below the grafting points (negative z), we add a reflective wall[19] at z = 0. The single layer of grafted PEO*n* is allowed to relax at constant volume and T = 300 K (NVT ensemble) for 5 ns. Since the goal is to mimic smectic order, as seen in 4T/PEO4,[9] after stabilizing the single grafted layer, we create a bilayer by replicating and inverting the single layer in the *z*-axis, thus making it nonperiodic in that direction and periodic in the *x*- and *y*-axis directions. This also results in an initial empty region between the two layers in the *z*-direction. On simulating the bilayer at 300 K for 500 ps under NVT conditions, we observe the value of the *z*-component of the pressure tensor, p_{zz}, to be negative due to the presence of interlayer vacuum. Since p_{zz} should be minimal when internal stresses are eliminated and approach zero (or 1 bar) when the layer thickness attains a mechanically stable thickness, we find the minimum value of p_{zz}^2 using the gradient descent method for varying interlayer separation. The distance between the layers (thickness) is changed by moving the grafting points and the reflective wall closer to each other in the *z*-axis, resulting in reduced volume due to the removal of the excess vacuum

https://dx.doi.org/10.1021/acsmacrolett.9b00935
ACS Macro Lett. 2020, 9, 295−300

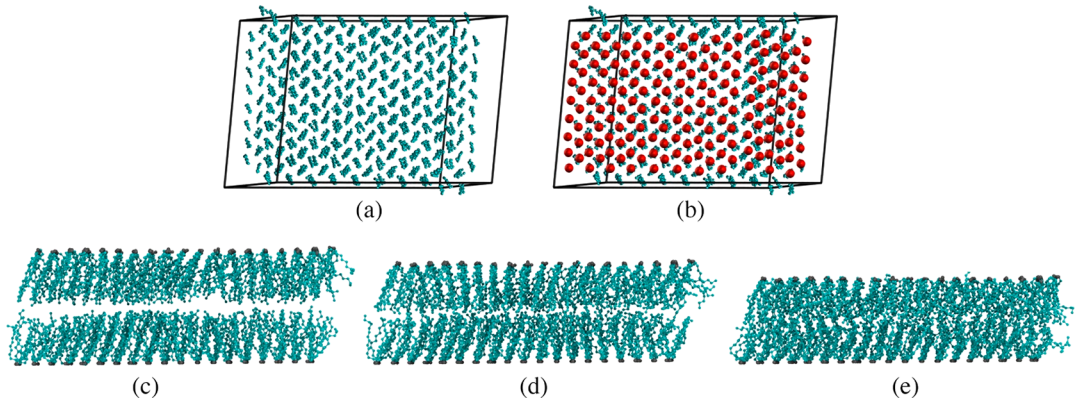

Figure 2. (a) Representative snapshot of 4T crystal from top view (*xy*-plane). (b) The red beads over the 4T crystal are the representative grafting sites for the PE or PEO chains. (c)−(e) Snapshots of the grafted PEO chains from the side view (*zx*-plane) as the vacuum in between is gradually reduced (at fixed *x*−*y* area); case (e) shows thermodynamically stable thickness when vacuum between the layers is removed and $P_{zz} = 0$.

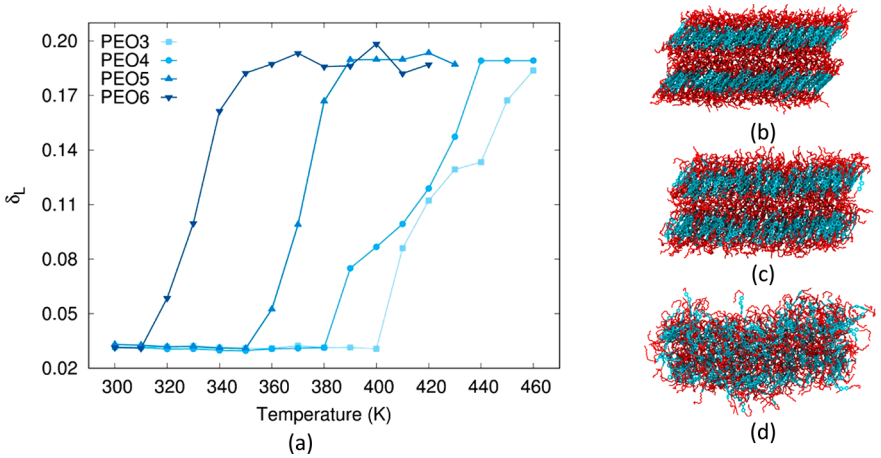

Figure 3. (a) Effect of temperature on the Lindemann Parameter for 4T/PEO*n* systems. Snapshot of configuration of 4T/PEO4 at $T = 350$ K (b), 390 K (c), and 440 K (d). The thiophene rings are shown in cyan, and the PEO units are shown in red; hydrogens are not shown.

(Figure 2). Note that the grafting points are not allowed to move in the *xy*-plane to maintain the "crystal order" (of the implicit 4T layer). The equilibrated bilayer thickness is seen to increase linearly with *n* for the two systems (Figure S2 in the SI). This linear correlation is characteristic of a strongly stretched regime for linear chains grafted on a flat surface, as reflected by the end-to-end distance values of the grafted chains in the *z*-direction (Figure S3 in the SI). In this regime, conformational changes (and the entropy generation) are more limited along the *z*-axis than along lateral (*x*−*y*) directions, resulting in increased lateral fluctuations of the chains around the mean position with an increase in *n*.[20−22]

To indirectly probe the increase in configurational entropy with chain length, we calculate the statistical average of the projected end-to-end distance of each oligomer on the *xy*-plane (R_{xy}) (Figure S4a in the SI). R_{xy} increases with *n* for both oligomers; however, PEO*n* increases more rapidly than PE*n*. To check if this disparity is related to the larger size of the PEO unit, we scaled *n* by the maximum possible length of the units in the all-trans state. Even after accounting for this size effect, we found that the trend persists (Figure S4b in the SI), indicative of higher configurational entropy in PEO*n* than in PE*n* chains for $n > 2$. Note that R_{xy} would be expected to scale as n^2 for self-avoiding chains grafted at a high GD on a flat surface;[23] however, since the *n* is small and we are operating in the highly stretched "rod-like" regime, we observe a linear scaling between R_{xy} and *n*. Figure 1(d) shows the $P2_1/a$ packing (primitive lattice with a 2-fold screw axis along *a*) of the thiophene rings with a nearest intermolecular distance between two α carbons of $p = 0.53$ nm. Note that the distance *p* is larger than the $\pi-\pi$ interaction distances of 0.39 and 0.44 nm as seen in our previous work.[9,18] Since *p* could be seen as a distance characterizing the ideal packing of 4T, the difference $(2R_{xy} - p)/p$ can be seen as a dimensionless metric of packing looseness "PL" at the given temperature. A positive and larger PL would be indicative of looser packing and hence larger lateral freedom and entropy. We hence hypothesize that for PL > 0 or $2R_{xy} > p$ the 4T packing may become destabilized. Note that PL > 0 need not guarantee instability of the smectic layer; rather, it would be a minimum threshold for it to happen. As seen in Figure 1(c), PL < 0 ($2R_{xy} < p$) for PE even with $n = 10$. However, a PL > 0 for PEO with $n = 5$ implies a tendency for instability of 4T/PEO*n* for $n \geq 5$ at the simulated temperature of 300 K (Figure 1a).

To test the hypothesis that the stability of the end-capped 4T systems can be estimated by calculating PL of grafted chains, we performed an all-atom simulation for 4T/PEO*n* at $n = 3$, 4, 5, and 6. Initial configurations are created using the final equilibrated PEO chains and reconstructing the 4T crystal structure from the grafted positions (Figure S1 in the SI). To map the thermal stability and morphological changes of 4T/PEO*n* systems, we heated sequentially the system from 300 to

https://dx.doi.org/10.1021/acsmacrolett.9b00935
ACS Macro Lett. 2020, 9, 295−300

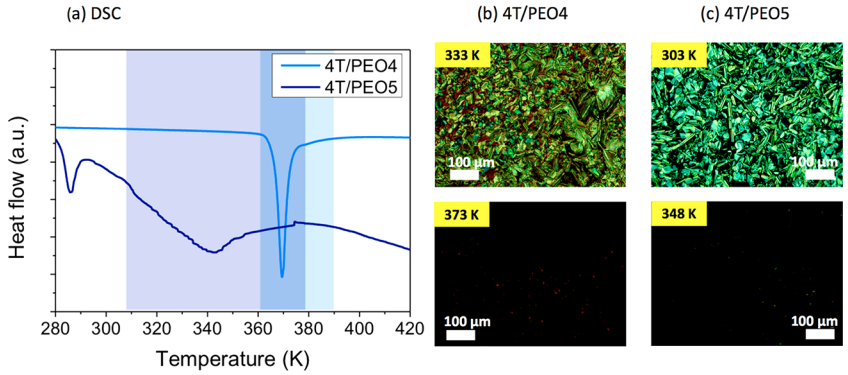

Figure 4. (a) Heating scans of DSC traces of 4T/PEO4 and 4T/PEO5 as a function of temperature. (b) and (c): POM images of 4T/PEO4 and 4T/PEO5 below (top row) and above (bottom row) order−disorder transition temperature. The scale bar is 100 μm.

460 K in 10 K increments. At each temperature, the system was annealed for 10 ns to try to achieve equilibrium before taking the next step and calculating densities and other material properties. On comparing the change of density with temperature (Figure S5 in the SI), we observed no abrupt changes that could be indicative of a first-order phase transition. However, visually we could observe an increase in the fluctuations of the molecular average positions, suggestive of melting. Hence, to try to detect when melting occurs, we calculated the Lindemann Parameter[24] (δ_L) for the thiophene rings, where δ_L is defined as the ratio of the root-mean-square fluctuation in atomic positions about the equilibrium lattice positions and the nearest-neighbor distance (p). Since in 4T/PEOn we want to capture the disordering of the smectic layer of thiophene rings, we measure δ_L for the center of mass of thiophene rings only. The threshold value for melting is generally considered as 15%, but it may vary between 5% and 20% depending on such factors as crystal structure, nature of interparticle interactions, and magnitude of nonclassical effects.[25] As shown in Figure 3(a), the critical value of δ_L for 4T/PEOn materials is around 5−10%, resulting in a melting point of 400, 380, 350, and 310 K for n = 3, 4, 5, and 6, respectively. Thus, the smectic order of 4T/PEO6 is found to be unstable near room-temperature conditions, consistent with the prediction of our earlier hypothesis based on the behavior of R_{xy} (PL) of the model-grafted bilayer system. These calculations are only intended to detect the onset of disordering (when δ_L increases rapidly) as the behavior of the curves for δ_L > 5−10% is largely uninformative. We also performed the same analysis for 4T/PEn for n = 3, 4, 5, and 6 and found the melting points to be higher than 380 K in each case (Figure S6 in the SI), consistent with available experimental data.[10] We further explored the effect of n on the potential energy between the components, and found results consistent with those obtained using the δ_L (Figures S7−9 in the SI).

To experimentally verify that the simulation results are capturing the correct trend in melting behavior with n, we also conducted the synthesis and characterization of 4T/PEO4 and 4T/PEO5 systems. We choose 4T/PEO5 for experimental characterization in addition to 4T/PEO4 since simulation predicted at 300 K 4T/PEOn undergoes order−disorder transition from n = 4 to n = 5 (Figure 1). The synthetic procedures of both compounds are shown in Figure S11 in the SI. At room temperature (near 300 K), 4T/PEO4 appears as a solid powder, whereas 4T/PEO5 appears as a sticky substance. The TGA curves (Figure S12a) suggest that both compounds remain thermally stable below 473 K, which is within the DSC temperature range (183−473 K) as shown in the heating cycle in Figure 4a. For 4T/PEO4, only a singular phase transition between smectic and isotropic melt shows up at around 367 K,[9] whereas for 4T/PEO5 a broader transition peak centered near 340 K is observed (indicated by the shaded areas). Such observations are consistent with the simulation trends of Figure 3 in that longer PEO chains result in lower melting point. The phases of both 4T/PEO4 and 4T/PEO5 were also characterized by POM. As can be seen in Figure 4b and 4c, fan-shaped textures, typical for smectic phases, are observed for both 4T/PEO4 and 4T/PEO5 at below the melting temperature, while black, featureless POM images are observed above the melting point for both compounds. This observation further supports that the transition temperature detected by DSC and simulation is indeed an LC order−disorder transition. To further verify that 4T crystallization controls the self-assembly behavior of 4T/PEOn systems, we employed T-dependent WAXS experiments to investigate both the $\pi-\pi$ interaction and smectic ordering of 4T/PEO4 and 4T/PEO5. Consistent with simulation results and DSC scans, we observe an order−disorder transition for 4T/PEO4 at 393 K and a broad transition for 4T/PEO5 centered around 350 K (Figure S14 in SI).

It has been a long-standing assumption that in this class of oligothiophenes, with terminal thiophene rings containing functionalized end-capping chains at their α-positions, the molecules would behave either like liquid crystals or like block copolymers depending on molecular weight.[26−29] However, our simulations paint a somewhat different and more nuanced picture. The smectic morphology observed here is primarily driven by the crystal structure of thiophene packing, while the functionalized groups at the end serve largely as space fillers between the ordered thiophene cores. This results in a nanosegregated two-domain structure where one domain is highly ordered and (nearly) crystalline (thiophene), while the other is less ordered and liquid-like (PEO capping groups). As the length of the capping chains increases, their associated increase in configurational entropy drives a tendency toward "liquidity" or disorder that eventually becomes comparable to the energetic attractive forces, keeping the ordered packing of the thiophene rings. This increased mobility of the capping chains "jiggles" the thiophene rings toward states of higher translational entropy and thus to the destabilization of their ordered packing. Because the ordered morphology is primarily governed by thiophene packing, to a first approximation the conformational behavior of the capping chains can be

https://dx.doi.org/10.1021/acsmacrolett.9b00935
ACS Macro Lett. 2020, 9, 295−300

computationally studied independently (as grafted chains in a bilayer) to efficiently identify trends with chain length, temperature, or other parameters. In the future, a similar approach could be used to efficiently test different chemical compositions of capping groups, calculating readily accessible properties as surrogates for the entropic forces driving the destabilization of the ordered domains (formed by thiophene or other units[30]). A rigorous approach to such tests would involve very expensive free-energy calculations to determine the melting behavior of each system of interest. The approximate approaches advocated here could be further extended to describe phases with different noncrystalline domain geometries[27] (besides a slab) and are hence expected to be a valuable addition to the toolbox used by simulators for a faster discovery of useful mixed ionic−electronic conducting materials.

■ ASSOCIATED CONTENT

Supporting Information

The Supporting Information is available free of charge at https://pubs.acs.org/doi/10.1021/acsmacrolett.9b00935.

Methodology for simulation details, Flory−Huggins parameter estimation, synthesis of 4T/PEO*n*, polarized optical microscopy (POM), and temperature-dependent wide-angle X-ray scattering (WAXS) data for 4T/PEO5. It also presents plots for the conformational properties of the grafted-chain system and the temperature dependence of the potential energy and structure factor of the full system (PDF)

■ AUTHOR INFORMATION

Corresponding Author

Fernando A. Escobedo − *School of Chemical and Biomolecular Engineering, Cornell University, Ithaca, New York 14853, United States;* orcid.org/0000-0002-4722-9836; Email: fe13@cornell.edu

Authors

Mayank Misra − *School of Chemical and Biomolecular Engineering, Cornell University, Ithaca, New York 14853, United States;* orcid.org/0000-0002-2700-1228

Ziwei Liu − *Materials Science and Engineering, Cornell University, Ithaca, New York 14853, United States*

Ban Xuan Dong − *Pritzker School of Molecular Engineering, University of Chicago, Chicago, Illinois 60637, United States;* orcid.org/0000-0002-2873-5207

Shrayesh N. Patel − *Pritzker School of Molecular Engineering, University of Chicago, Chicago, Illinois 60637, United States; Chemical Science and Engineering Division, Argonne National Laboratory, Lemont, Illinois 60439, United States;* orcid.org/0000-0003-3657-827X

Paul F. Nealey − *Pritzker School of Molecular Engineering, University of Chicago, Chicago, Illinois 60637, United States; Materials Science Division, Argonne National Laboratory, Lemont, Illinois 60439, United States;* orcid.org/0000-0003-3889-142X

Christopher K. Ober − *Materials Science and Engineering, Cornell University, Ithaca, New York 14853, United States;* orcid.org/0000-0002-3805-3314

Complete contact information is available at: https://pubs.acs.org/10.1021/acsmacrolett.9b00935

Notes

The authors declare no competing financial interest.

■ ACKNOWLEDGMENTS

The authors acknowledge financial support from the National Science Foundation under Contract No. DMREF-1922259. The simulations were performed on Comet-GPU on XSEDE using the grant TG-CTS180023. This work made use of the Cornell Center for Materials Research Shared Facilities, which are supported through the NSF MRSEC program.

■ REFERENCES

(1) Gkoupidenis, P.; Schaefer, N.; Garlan, B.; Malliaras, G. G. Neuromorphic Functions in PEDOT:PSS Organic Electrochemical Transistors. *Adv. Mater.* **2015**, *27* (44), 7176−7180.

(2) Kaihovirta, N.; Mäkelä, T.; He, X.; Wikman, C.-J.; Wilén, C.-E.; Österbacka, R. Printed All-Polymer Electrochemical Transistors on Patterned Ion Conducting Membranes. *Org. Electron.* **2010**, *11* (7), 1207−1211.

(3) Tarabella, G.; D'Angelo, P.; Cifarelli, A.; Dimonte, A.; Romeo, A.; Berzina, T.; Erokhin, V.; Iannotta, S. A Hybrid Living/Organic Electrochemical Transistor Based on the Physarum Polycephalum Cell Endowed with Both Sensing and Memristive Properties. *Chem. Sci.* **2015**, *6* (5), 2859−2868.

(4) Malti, A.; Edberg, J.; Granberg, H.; Khan, Z. U.; Andreasen, J. W.; Liu, X.; Zhao, D.; Zhang, H.; Yao, Y.; Brill, J. W.; Engquist, I.; Fahlman, M.; Wågberg, L.; Crispin, X.; Berggren, M. An Organic Mixed Ion-Electron Conductor for Power Electronics. *Adv. Sci.* **2016**, *3* (2), 1500305.

(5) Kim, S. H.; Hong, K.; Xie, W.; Lee, K. H.; Zhang, S.; Lodge, T. P.; Frisbie, C. D. Electrolyte-Gated Transistors for Organic and Printed Electronics. *Adv. Mater.* **2013**, *25* (13), 1822−1846.

(6) Bhatt, M. P.; Thelen, J. L.; Balsara, N. P. Effect of Copolymer Composition on Electronic Conductivity of Electrochemically Oxidized Poly(3-Hexylthiophene)- *b* -Poly(Ethylene Oxide) Block Copolymers. *Chem. Mater.* **2015**, *27* (14), 5141−5148.

(7) He, L.; Pan, S.; Peng, J. Morphology Control of Poly(3-Hexylthiophene)- *b* -Poly(Ethylene Oxide) Block Copolymer by Solvent Blending. *J. Polym. Sci., Part B: Polym. Phys.* **2016**, *54* (5), 544−551.

(8) Dong, B. X.; Nowak, C.; Onorato, J. W.; Strzalka, J.; Escobedo, F. A.; Luscombe, C. K.; Nealey, P. F.; Patel, S. N. Influence of Side-Chain Chemistry on Structure and Ionic Conduction Characteristics of Polythiophene Derivatives: A Computational and Experimental Study. *Chem. Mater.* **2019**, *31* (4), 1418−1429.

(9) Liu, Z.; Dong, B. X.; Misra, M.; Sun, Y.; Strzalka, J.; Patel, S. N.; Escobedo, F. A.; Nealey, P. F.; Ober, C. K. Self-Assembly Behavior of An Oligothiophene-Based Conjugated Liquid Crystal and Its Implication for Ionic Conductivity Characteristics. *Adv. Funct. Mater.* **2019**, *29*, 1805220.

(10) Ashizawa, M.; Niimura, T.; Yu, Y.; Tsuboi, K.; Matsumoto, H.; Yamada, R.; Kawauchi, S.; Tanioka, A.; Mori, T. Improved Stability of Organic Field-Effect Transistor Performance in Oligothiophenes Including *β*-Isomers. *Tetrahedron* **2012**, *68* (13), 2790−2798.

(11) Damman, P.; Paternostre, L.; Moulin, J.-F.; Dosiere, M. Crystal Structure of Poly (Ethy1ene-Oxide) Supramolecular Assemblies. *Macromol. Symp.* **1999**, *138*, 57−71.

(12) Liu, G.; Baker, G. L. Structure-Directed Self-Assembly of Alkyl-Aryl-Ethylene Oxide Amphiphiles. *Soft Matter* **2008**, *4* (5), 1094−1101.

(13) Sperling, L. H. *Introduction to Physical Polymer Science*; John Wiley & Sons, Inc.: Hoboken, NJ, USA, 2005.

(14) Caddeo, C.; Mattoni, A. Atomistic Investigation of the Solubility of 3-Alkylthiophene Polymers in Tetrahydrofuran Solvent. *Macromolecules* **2013**, *46* (19), 8003−8008.

(15) Plimpton, S. Fast Parallel Algorithms for Short-Range Molecular Dynamics. *J. Comput. Phys.* **1995**, *117* (1), 1−19.

(16) Min, C. Electroactive Thermoplastic Dielectric Elastomers as a New Generation Polymer Actuators. In *Thermoplastic Elastomers*; InTech, 2012.
(17) Yao, Z. F.; Wang, J. Y.; Pei, J. Control of π-π Stacking via Crystal Engineering in Organic Conjugated Small Molecule Crystals. *Cryst. Growth Des.* **2018**, *18* (1), 7−15.
(18) Dong, B. X.; Liu, Z.; Misra, M.; Strzalka, J.; Niklas, J.; Poluektov, O. G.; Escobedo, F. A.; Ober, C. K.; Nealey, P. F.; Patel, S. N. Structure Control of a π-Conjugated Oligothiophene-Based Liquid Crystal for Enhanced Mixed Ion/Electron Transport Characteristics. *ACS Nano* **2019**, *13*, 7665−7675.
(19) Bond, S.; Leimkuhler, B. Stabilized Integration of Hamiltonian Systems with Hard-Sphere Inequality Constraints. *SIAM J. Sci. Comput.* **2008**, *30* (1), 134−147.
(20) Dimitrov, D.; Milchev, A.; Binder, K. Polymer Brushes on Flat and Curved Substrates: Scaling Concepts and Computer Simulations. *Macromol. Symp.* **2007**, *252* (1), 47−57.
(21) Nair, N.; Wentzel, N.; Jayaraman, A. Effect of Bidispersity in Grafted Chain Length on Grafted Chain Conformations and Potential of Mean Force between Polymer Grafted Nanoparticles in a Homopolymer Matrix. *J. Chem. Phys.* **2011**, *134* (19), 194906.
(22) Dukes, D.; Li, Y.; Lewis, S.; Benicewicz, B.; Schadler, L.; Kumar, S. K. Conformational Transitions of Spherical Polymer Brushes: Synthesis, Characterization, and Theory. *Macromolecules* **2010**, *43* (3), 1564−1570.
(23) Kirk, J.; Ilg, P. Chain Dynamics in Polymer Melts at Flat Surfaces. *Macromolecules* **2017**, *50* (9), 3703−3718.
(24) Lindemann, F. A. The Calculation of Molecular Vibration Frequencies. *Phys. Z.* **1910**, *11* (11), 609−612.
(25) Chakravarty, C.; Debenedetti, P. G.; Stillinger, F. H. Lindemann Measures for the Solid-Liquid Phase Transition. *J. Chem. Phys.* **2007**, *126* (20), 204508.
(26) Sasaki, K.; Shibata, Y.; Lu, M.; Yoshida, Y.; Azumi, R.; Ueda, Y. Effect of Side Chain of Oligothiophene Derivatives on Bulk Heterojunction Structure in Organic Photovoltaic Devices. *Adv. Mater. Phys. Chem.* **2013**, *03* (02), 185−190.
(27) Sun, Y.; Padmanabhan, P.; Misra, M.; Escobedo, F. A. Molecular Dynamics Simulation of Thermotropic Bolaamphiphiles with a Swallow-Tail Lateral Chain: Formation of Cubic Network Phases. *Soft Matter* **2017**, *13* (45), 8542.
(28) Zhang, L.; Colella, N. S.; Cherniawski, B. P.; Mannsfeld, S. C. B.; Briseno, A. L. Oligothiophene Semiconductors: Synthesis, Characterization, and Applications for Organic Devices. *ACS Appl. Mater. Interfaces* **2014**, *6* (8), 5327−5343.
(29) Kaloni, T. P.; Giesbrecht, P. K.; Schreckenbach, G.; Freund, M. S. Polythiophene: From Fundamental Perspectives to Applications. *Chem. Mater.* **2017**, *29* (24), 10248−10283.
(30) Escobedo, F. A.; Chen, Z. Liquid Crystalline Behavior of a Semifluorinated Oligomer. *J. Chem. Phys.* **2004**, *121* (22), 11463−11473.

https://dx.doi.org/10.1021/acsmacrolett.9b00935
ACS Macro Lett. 2020, 9, 295−300